*Pure Appl. Chem.*, Vol. 76, No. 9, pp. 1647–1658, 2004.


# Design of composite micro/mesoporous molecular sieve catalysts*

Irina I. Ivanova‡, Andrei S. Kuznetsov, Valentina V. Yuschenko, and Elena E. Knyazeva

*Department of Chemistry, Moscow State University, Lenin Hills, Moscow 119992, Russia*

*Abstract*: Two series of composite micro/mesoporous materials with different contributions of micro- and mesoporosity were prepared by dealumination and recrystallization of mordenite zeolite. The materials were characterized by X-ray diffraction, infrared spectroscopy, $^{27}$Al magic angle spinning (MAS) NMR, nitrogen adsorption–desorption, and temperature-programmed desorption of ammonia (TPD $NH_3$). Catalytic properties were studied in transalkylation of biphenyl with diisopropylbenzene. Both types of composite materials showed remarkably high activity, stability, and selectivity toward formation of diisopropylbiphenyls with respect to both pure microporous and mesoporous materials. The effect is due to high zeolitic acidity combined with improved accessibility of active sites and transport of bulky molecules provided by mesopores.

## INTRODUCTION

Microporous molecular sieves, such as zeolites and zeolite-like materials, are among the most important heterogeneous catalysts, due to their strong acidity, good thermal and hydrothermal stability, and unique molecular shape selectivity. However, due to the limited size of zeolites pores (<1 nm), they cannot be used in the processing of larger molecules. The appearance of mesoporous molecular sieves in 1992 [1,2] was considered as a great challenge in heterogeneous catalysis, since it was expected that they could be applied for the conversion of bulky molecules. In particular, it was anticipated that they would find application in refinery for deep catalytic cracking, as well as in fine chemistry for production of pharmaceuticals. However, as revealed by subsequent studies, their rather low stability in the presence of water vapor and comparatively low acidity did not allow them to satisfy the requirements for the above-mentioned processes and none of these materials has been commercialized as yet.

It was thus very attractive to design the materials, which will combine the advantages of both mesoporous molecular sieves and zeolites. Two approaches can be used for the design of such kinds of systems. The first approach is based on the creation of mesopores in the crystals of zeolites, while the second involves building of mesoporous materials from tiny zeolitic species.

The methodologies used for the preparation of mesoporous zeolite single crystals involve conventional dealumination procedures, such as steaming, acid, and alkaline treatments [3–5], or matrix-assisted synthesis, reported recently by Jacobsen et al. [6]. In the latter case, mesoporous carbon matrix was impregnated with reaction mixture for zeolite ZSM-5 synthesis, and zeolite crystals were grown around the carbon particles. The removal of encapsulated carbon matrix by calcination led to isolated large zeolite crystals with uniform mesopore system.

---

*Plenary lecture presented at the XVII Mendeleev Congress on General and Applied Chemistry, Kazan, Tatarstan, Russia, 21–26 September 2003. Other presentations are published in this issue, pp. 1605–1798.

‡Corresponding author: E-mail: IIIvanova@phys.chem.msu.ru

For the design of mesoporous materials from tiny zeolitic species, the first strategy was to use simultaneously the large surfactant as a template for creating mesopores and a small organic template for building zeolitic microporous units. This dual template strategy has been tested in [7]. The materials obtained showed enhanced stability and acidity with respect to mesoporous materials, but the results of scanning electron microscopy (SEM) studies demonstrated that they represent a physical mixture of zeolite and mesoporous material instead of homogeneous material. Two templates were thus working competitively instead of cooperatively.

A different result was obtained when the synthesis was carried out in two steps. In the first step, tiny zeolite seeds were prepared by the short hydrothermal step and then the second hydrothermal reaction was performed after adding surfactant, required for the synthesis of mesoporous material [8–15]. The authors [10] believe that such materials involve ordered mesostructures with zeolite-like subunits of $AlO_4$ and $SiO_4$ tetrahedra in the walls. The evidence for the retention of the protozeolitic connectivity of tetrahedra was provided by IR spectroscopy.

The other procedure used for the preparation of tiny zeolite fragments involves partial dissolution of zeolites in highly alkaline media [16]. The authors suggest that the fragments formed at the dissolution step are further tailored during recrystallization step into mesostructure.

The opposite strategy followed by the groups of Van Bekkum [17] and Kaliaguine [18,19], included transformation of the preassembled walls of mesoporous materials such as MCM-41 and SBA-15 into zeolitic structures by postassembly treatment with zeolite structure-directing template. The wall of such material was indeed partially crystallized into zeolite, as it was evidence of transmission electron microscopy (TEM) images showing small zeolite crystals embedded in the walls of mesoporous materials. However, this approach allowed us to achieve only low degrees of crystallinity not higher than 40 %. Further crystallization resulted in extra-wall growth of zeolite crystals and finally destroyed the mesoporous structure.

A slightly different approach also adopted by Kaliaguine and coworkers [20] included coating of mesoporous materials with nanozeolite seeds using very diluted clear zeolite gels. Basing on TEM results, the authors supposed that such coating procedure leads to grafting nanoclastered zeolite particles on the walls of mesopores by condensation of silanols at the interface.

Another type of material with micropore walls or micropore walls combined with microporous plugs was obtained by Inagaki [21] and Voort [22], respectively, by adjusting temperature and tetraethoxysilan/surfactant ratio during the synthesis of SBA-15. Although the walls of these materials were shown to be microporous, they were not crystalline.

A very interesting strategy for the synthesis of micro/mesoporous materials was adopted by Corma and coworkers [23]. They explored the possibility of formation of delaminated zeolites. The procedure was based on swelling of the layers of zeolite precursor by alkylammonium bromide. The exfoliation or separation of such swelled layers by ultrasound, freeze-drying, or vigorous stirring led to materials with randomly oriented zeolitic layers or pillared in face-to-face orientation. It should be noted that mesopores were not ordered in these materials.

The analysis of the literature data on the micro/mesoporous composites suggest that in most of the cases these materials show enhanced stability and acidity with respect to mesoporous materials. In some cases, there are also evidences for the enhanced catalytic activity. However, the information on the catalytic properties of such materials is very limited.

Herein, we present the results on the catalytic activity of two types of micro/mesoporous composite solids based on zeolite single crystals with secondary mesoporous structure and mesoporous materials composed of tiny zeolitic species. Dealumination [24] and recrystallization [16] procedures were used for the preparation of these materials, respectively. Transalkylation of biphenyl and 1,4-diisopropylbenzene was selected as model reaction.

## EXPERIMENTAL

### Preparation of composite micro/mesoporous materials from mordenites

The starting mordenites CBV10 and CBV90 were supplied by Zeolyst. CBV10 was a parent synthetic zeolite in H-form with *Si/Al* = 7.6, while CBV90 was a dealuminated mordenite with *Si/Al* = 49. In this contribution, CBV10 was assigned as MOR(8) and CBV90 as De-MOR(49).

MOR(8) was further dealuminated by calcination at 750 °C followed by acid attack. Oxalic and methanesulfonic acids were used for acidic treatments. Both procedures led to higher degrees of dealumination than in the case of commercially dealuminated sample, De-MOR(49). Thus, treatment with oxalic acid resulted in the increase of *Si/Al* ratio up to 320, while methanesulfonic acid led to the *Si/Al* ratio of 80. The samples prepared were assigned as De-MOR(320) and De-MOR(80), respectively.

The recrystallized mordenites Re-MOR 1, Re-MOR 2, and Re-MOR 3 were obtained from De-MOR(49) sample using two-step procedure including partial destruction of mordenite in NaOH aqueous solution, followed by its hydrothermal treatment in the presence of cethyltrimethylammonium bromide at 373 K. In the series of samples prepared, the concentration of NaOH was 0.3, 0.7, and 1.6 M, respectively. More detailed procedure for mordenites recrystallization was described in [16].

### Characterization

The elemental analyses of dealuminated mordenites was performed by atomic absorption. The XRD patterns were obtained with a DRON-3M diffractometer using Cu Kα radiation. Fourier transform infrared (FTIR) spectra were recorded with a Nicolet Protege 460 IR spectrometer. $^{27}$Al MAS NMR experiments were performed on a Bruker MSL 400 spectrometer ($\nu\,^{27}$Al = 104.3 MHz). The spectra were recorded with π/12 pulse length of 1 μs, a recycle delay of 0.2 s, and spinning rate of 10 kHz. The chemical shifts were referenced to $Al(NO_3)_3$.

Sorption–desorption isotherms of nitrogen were measured at 77 K using an automated porosimeter (Micromeritics ASAP 2000). Micropore volumes were determined using t-plot method. The total sorbed volumes, including adsorption in the micropores and mesopores and on the external surface, were calculated from the amount of nitrogen adsorbed at relative pressure $p/p_0$ of 0.96, before the onset of interparticle condensation.

The acidic properties were studied by temperature-programmed desorption of ammonia ($NH_3$–TPD). $NH_3$–TPD was performed in a home-made set-up equipped with TC detector. Prior to $NH_3$ adsorption, the samples were calcined in situ in a flow of dry air at 823 K for 1 h and, subsequently, in a flow of dry nitrogen for 1 h and cooled down to ambient temperature. The $NH_3$ adsorption was carried out during 30 min, at ambient temperature in a flow of $NH_3$ diluted with $N_2$ (1/1). Subsequently, the physisorbed $NH_3$ was removed in a flow of dry He at 373 K for 1 h. Typical TPD experiments were carried out in the temperature range of 295 to 1055 K in a flow of dry He (30 ml/min.). The rate of heating was 8 K/min.

### Catalytic testing

Transalkylation of biphenyl (BP) with 1,4-diisopropylbenzene (1,4-DIPB) was carried out in a fixed-bed flow reactor under 1 MPa. The reaction temperature was 493 K. The weight hourly space velocity of biphenyl ($WHSV_{BP}$) was 0.5 $h^{-1}$. The reaction was carried out in dry $N_2$ as a carrier gas, the molar ratio *BP:DIPB:*$N_2$ was 1:5:10. The analysis of reaction products was carried out by gas chromatography (GC) using 50 m capillary column SE-30.

## RESULTS AND DISCUSSION

### Dealuminated mordenites

The main characteristics of the parent, MOR(8), and dealuminated De-MOR(49), De-MOR(80), and De-MOR(320) zeolites are presented in Table 1 and Figs. 1–3. The results show that the procedures selected for dealumination in this study allowed for gradual increase of the *Si/Al* ratio from 7.6 to 320. X-ray diffraction (XRD) and infrared (IR) data confirmed the preservation of mordenite structure after dealumination in all the samples studied. $^{27}$Al MAS NMR spectra presented in Fig. 1 contained only the signals corresponding to tetrahedrally coordinated framework aluminum. All the extra-framework aluminum species were removed from the samples upon acidic treatments.

**Table 1** Characteristics of parent and dealuminated mordenites.

| Samples | *Si/Al* | *S*, $m^2/g$ | *V*, $cm^3/g$ | $V_{mic}$, $cm^3/g$ | $a_o$*, μmol/g |
|---|---|---|---|---|---|
| MOR(8) | 7 | 320 | 0.175 | 0.135 | 1320 |
| De-MOR(320) | 320 | 545 | 0.295 | 0.207 | 70 |
| De-MOR(80) | 80 | 590 | 0.297 | 0.197 | 150 |
| De-MOR(49) | 48 | 425 | 0.245 | 0.160 | 240 |

*Concentration of acid sites determined by $NH_3$ TPD.

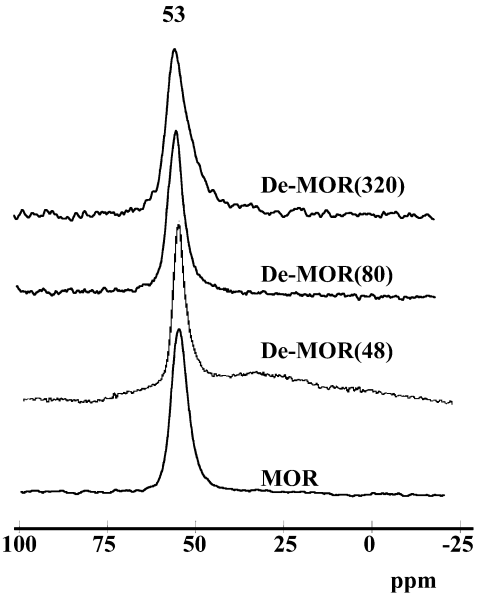


**Fig. 1** $^{27}$Al MAS NMR spectra of parent and dealuminated mordenites.

While the structure of mordenite as well as the state and location of residual aluminum ions did not change upon dealumination, its texture underwent significant changes (Fig. 2). The parent zeolite, MOR(8), showed reversible type-I adsorption/desorption isotherm with a steep rise at $p/p_0 < 0.01$, typical for microporous solid. The isotherms of the three other samples exhibited irreversible type IV isotherms with a hysteresis loop at a lower closing point at $p/p_0 = 0.42$, indicating the formation of mesopores with broad distribution of sizes.

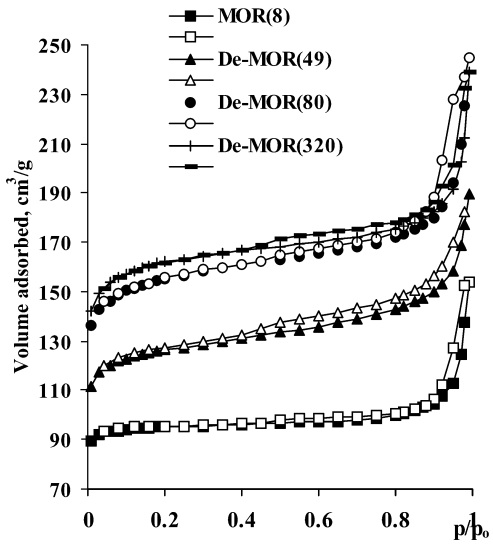


**Fig. 2** Nitrogen adsorption/desorption isotherms obtained at 77 K over parent and dealuminated mordenites.

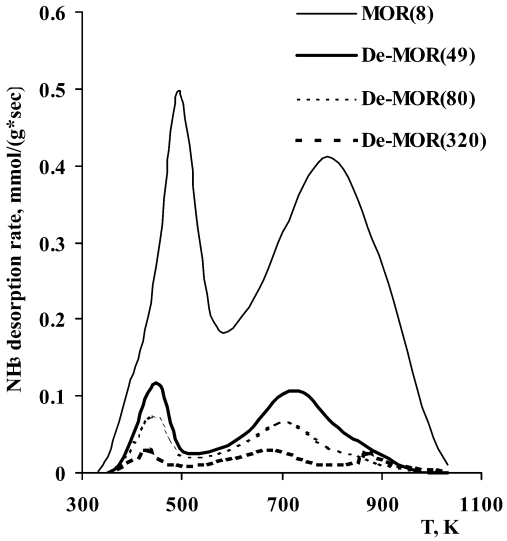


**Fig. 3** $NH_3$–TPD patterns over parent and dealuminated mordenites.

The pore volumes of the various samples are reported in Table 1 and point to the following changes occurring upon dealumination:

- dealumination up to *Si/Al* = 49 (commercially dealuminated sample) leads to the increase of both, micro- and mesopore volumes;
- dealumination using methanesulfonic acid leading to *Si/Al* = 80 further increases micro- and mesopore volumes.
- However, deeper dealumination up to *Si/Al* = 320 using oxalic acid does not result in further increase of the volumes of micro- and mesopores.

Consequently, there exists a limit, after which the removal of aluminum does not lead to creation of new pores.

The number of acidic sites in the samples, measured by TPD $NH_3$ is given in the last column of Table 1. As expected, it decreases with the increase of *Si/Al* ratio upon dealumination. On the contrary, the acid site distribution does not change significantly with the degree of dealumination. Practically all the TPD-$NH_3$ spectra contained low temperature peak and high temperature peak with a shoulder at higher temperatures. The gradual decrease of the temperatures of TPD maxima with the increase of *Si/Al* ratio in the samples is most probably due to easier diffusion of $NH_3$ adsorbed on dealuminated samples.

The catalytic properties were studied in transalkylation of BP and 1,4-DIPB. The results are presented in Table 2. The major products of biphenyl conversion were isopropylbiphenyl (IPBP), diisopropylbiphenyl (DIPBP), as well as small amounts of polyalkylbiphenyls ($C_{18}$+ and Other). Besides alkylbiphenyls, quaterphenyls (QPs) were observed in smaller amounts. The main products of 1,4-DIPB conversion were cumene, benzene as well as IPBP and DIPBP; triisopropylbenzenes and alkylbiphenyls were observed in smaller amounts. Besides transalkylation, 1,4-DIPB was found to undergo isomerization towards ortho- and meta-DIPB, meta-DIPB being the major product of isomerization. Among all the products formed, DIPBP were the target products, since they can be further used in the synthesis of advanced polymer materials with high thermal and mechanical stability or thermotropic liquid-crystal properties.

**Table 2** Transalkylation of biphenyl and 1,4-diisopropylbenzene over parent and dealuminated mordenites ($T$ = 220 °C, $WHSV_{BP}$ = 0.5 $h^{-1}$, $p$ = 1 MPa, *BP:DIPB:*$N_2$ = 1:5:10 mol.).

| Catalyst | MOR(8) | De-MOR(49) | De-MOR(80) | De-MOR(320) |
|---|---|---|---|---|
| Conversion (%) of | | | | |
| BP | 17.9 | 24.7 | 57.1 | 34.6 |
| DIPB | 3.0 | 3.7 | 18.8 | 6.5 |
| Selectivity to BP products (%) | | | | |
| IPBP | 42.1 | 37.8 | 35.9 | 44.6 |
| DIPBP | 5.8 | 17.9 | 46.0 | 35.4 |
| $C_{18}$+ | 10.2 | 5.4 | 3.6 | 3.6 |
| QP | 36.6 | 18.9 | 3.4 | 6.2 |
| Other | 5.3 | 19.9 | 11.1 | 10.2 |

The parent mordenite, MOR(8), showed rather low conversion of 1,4-DIPB and BP (Table 2). The main reaction pathway over this catalyst was transalkylation of BP and 1,4-DIPB leading to IPBP. Besides that, the formation of QP occurred in rather large extent. The latter was probably responsible for very fast catalyst deactivation in the beginning of the reaction over this catalyst.

Dealumination of parent mordenite up to *Si/Al* ratio of 80 led to gradual increase of BP and 1,4-DIPB conversion and selectivity to DIPB products. Meanwhile, selectivity to QP decreased tremendously and the stability of the catalytic activity increased (Table 2). These observations could hardly be explained by the changes in acidity upon dealumination and are most probably due to formation of secondary porous system, which allows for better accessibility of active sites for the reactants and easier transport of bulky products from the porous system of mordenite.

Further dealumination up to *Si/Al* ratio of 320, which did not result in creation of new pores with respect to De-MOR(80), led to some decrease of the conversion. Meanwhile, the selectivity did not change significantly. This effect could be due to the decrease of the amount of acid sites.

To summarize, the comparative study of parent and dealuminated mordenites in transalkylation of BP with 1,4-DIPB pointed to remarkable activity of dealuminated mordenites with respect to the starting mordenite. The results suggest that the catalytic activity, selectivity, and stability of dealuminated mordenites in transalkylation is governed by the formation of a secondary porous network interconnecting micropores, which allows for acid site accessibility, facilitates the transport of bulky reactants and products, and prevents deactivation by pore blocking. The best result was obtained over De-MOR(80) with the highest pore volume and rather high residual amount of acid sites.

## Recrystallized mordenites

The starting mordenite used for recrystallization was De-MOR(49). The results presented in Table 3 show that recrystallization of De-MOR(49) have not affected the chemical composition of the sample. On the contrary, the structure and texture of recrystallized samples were affected significantly by the conditions of recrystallization, in particular, the concentration of NaOH solution taken for zeolite destruction was the most important parameter (Table 3, Figs. 4–7).

**Table 3** Characteristics of parent and recrystallized mordenites.

| Samples | *Si/Al* | $V$, $cm^3/g$ | $V_{mic}$, $cm^3/g$ | $d_{meso}$, A | $a_o$*, μmol./g |
|---|---|---|---|---|---|
| De-MOR(49) | 49 | 0.245 | 0.160 | - | 365 |
| Re-MOR 1 | 46 | 0.400 | 0.147 | 30 | 322 |
| Re-MOR 2 | 47 | 0.660 | 0.080 | 30 | 311 |
| Re-MOR 3 | 47 | 0.918 | 0.017 | 30 | 130 |

*Concentration of acid sites determined by $NH_3$ TPD.

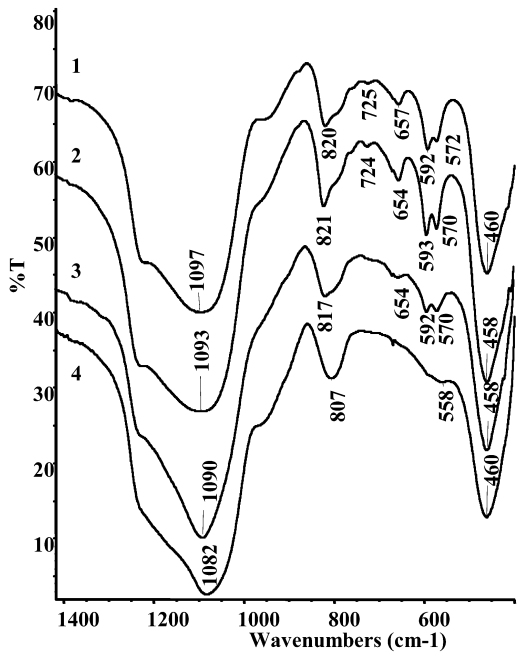


**Fig. 4** IR spectra of starting mordenite De-MOR(49) (1) and recrystallized samples Re-MOR 1 (2), Re-MOR 2 (3), Re-MOR 3 (4).

The results of a FTIR study showed that the destruction of starting mordenite in 0.3 and 0.7 M solutions does not affect significantly the crystallinity of recrystallized mordenites (Fig. 4). In the case of the Re-MOR 1, the bands at 570 and 592 $cm^{-1}$ corresponding to stretching vibrations became even more intensive and sharper. On the contrary, destruction in 1.6 M solution led to disappearance of these bands. XRD data confirmed the results obtained by FTIR (Fig. 5). On Re-MOR 2, only a small halo in the region of 15–20 2θ due to amorphous material was observed, while on Re-MOR 3, the peaks corresponding to mordenite phase practically disappeared and the broad halo gave the main contribution to the XRD pattern. The XRD data recorded in the region of 5–50 2θ did not allow to verify, whether observation of amorphous phase was due to formation of mesoporous material.

This information was obtained from the isotherms of $N_2$ adsorption–desorption. Figure 6 shows that recrystallized mordenites exhibit rather sharp steps at $p/p_0 \sim 0.35$, corresponding to the existence of uniform mesopores. The horizontal hysteresis loop after $p/p_0 \sim 0.45$ further suggested the existence of secondary texture mesopores. According to BJH calculation, the size of the mesopores was about 3.0 nm. The formation of mesopores resulted in significant increase of pore volumes of the samples

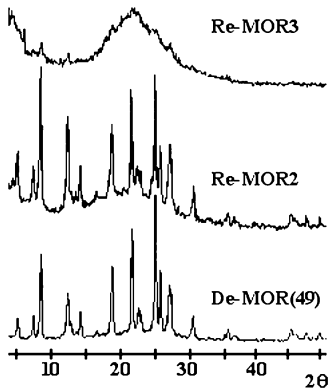


**Fig. 5** XRD patterns of starting mordenite De-MOR(49) and recrystallized samples Re-MOR 2, Re-MOR 3.

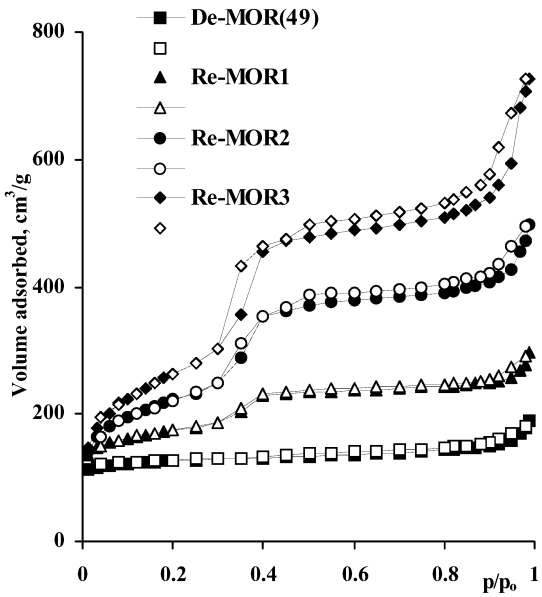


**Fig. 6** Nitrogen adsorption/desorption isotherms obtained at 77 K over starting and recrystallized mordenites.

upon recrystallization (Table 3). It should be noted that the higher was the concentration of NaOH solution used for zeolite destruction, the higher was the growth in mesopore volume. On the contrary, the micropore volume decreased with the concentration of NaOH solution used for zeolite destruction. This suggests that the degree of recrystallization of mordenite into mesoporous material can be adjusted by variation of the concentration of NaOH in solution.

In $^{27}$Al MAS NMR spectra (Fig. 7), the peaks around 53 and 13 ppm were indicative of tetrahedrally coordinated aluminum in the framework and octahedral aluminum, respectively. The starting mordenite De-MOR(49) exhibited mostly tetrahedrally coordinated framework aluminum. Recrystallization leads to the decrease of the intensity of the peak of tetrahedrally coordinated aluminum and appearance of the peak corresponding to octahedral aluminum. The contribution of octahedral state of aluminum gradually increased with the degree of recrystallization.

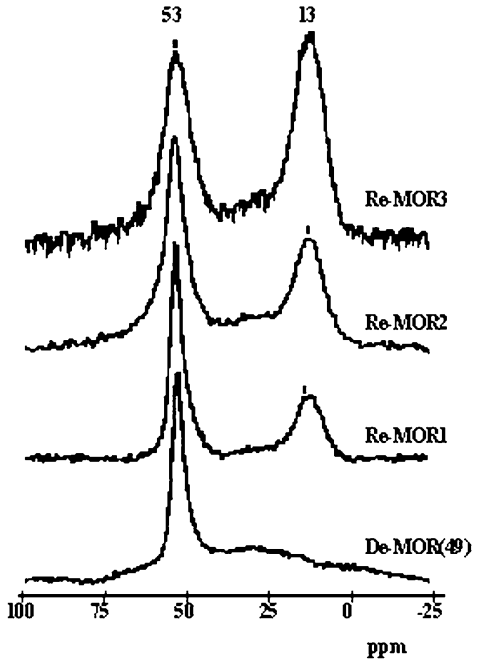


**Fig. 7** $^{27}$Al MAS NMR spectra of parent and recrystallized mordenites.

It is interesting that TPD $NH_3$ results over recrystallized samples showed that the samples Re-MOR 1 and Re-MOR 2 exhibited strong acidity. On Re-MOR 1, the amount of strong acid sites was even higher than on parent mordenite (Fig. 8). This suggests that these materials are not simply a mixture of mordenite and mesoporous material. On the contrary, the TPD profile for the sample Re-MOR 3 was quite different: the contribution of weak and strong sites decreased significantly, while the amount of medium sites remained the same. Such TPD $NH_3$ profile corresponds to amorphous sample. The total amount of sites on Re-MOR 1 and Re-MOR 2 was similar to starting mordenite, while on Re-MOR 3 it decreased by a factor of 3 (Table 3).

The catalytic results obtained over recrystallized mordenites in transalkylation of BP with 1,4-DIPB are presented in Table 4. The properties of starting mordenite De-MOR(49) and purely mesoporous catalyst MCM-41 are given for comparison. Recrystallization of De-MOR(49) into Re-MOR 1 and Re-MOR 2 led to 2–3-fold increase of BP conversion and 6–7-fold increase of the conversion of 1,4-DIPB with respect to starting mordenite. Furthermore, it resulted in the increase of the selectivity toward DIPBPs, while selectivity to QP decreased several times. Consequently, composite micro/mesoporous materials possess improved catalytic properties with respect to both microporous and meso-

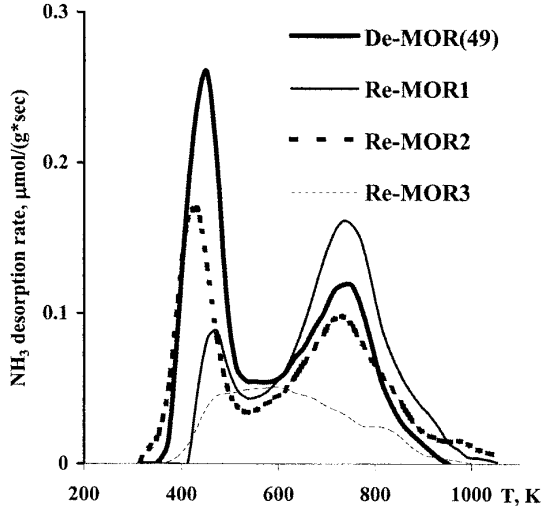


**Fig. 8** $NH_3$ TPD patterns over parent and recrystallized mordenites.

porous materials, again suggesting that they are not a physical mixture of mordenite and mesoporous material. On the other hand, deeper recrystallization into Re-MOR 3, exhibiting the properties of purely mesoporous material, led to very low catalytic activity, comparable with MCM-41 catalyst (Table 4).

**Table 4** Transalkylation of biphenyl and 1,4-diisopropylbenzene over recrystallized mordenites ($T$ = 220 °C, $WHSV_{BP}$ = 0.5 $h^{-1}$, $p$ = 1 MPa, $BP:DIPB:N_2$ = 1:5:10 mol.).

| Catalyst | De-MOR(49) | Re-MOR 1 | Re-MOR 2 | Re-MOR 3 | MCM-41 |
|---|---|---|---|---|---|
| Conversion of (%) | | | | | |
| BP | 24.7 | 69.1 | 54.5 | 15.2 | 23.6 |
| DIPB | 3.7 | 24.9 | 22.3 | 5.4 | 14.7 |
| Selectivity to BP products (%) | | | | | |
| IPBP | 37.8 | 34.7 | 42.4 | 43.7 | 73.4 |
| DIPBP | 17.9 | 47.1 | 39.1 | 2.5 | 6.7 |
| $C_{18}$+ | 5.4 | 5.1 | 9.7 | 12.4 | 4.2 |
| QP | 18.9 | 4.6 | 0.7 | 34.8 | 2.6 |
| Other | 19.9 | 8.4 | 8.2 | 6.6 | 13.1 |

The analysis of the structural, acidic, and catalytic properties of recrystallized mordenites suggests that after dissolution step, the fragments of mordenite existing in solution are further tailored to mesostructure, giving composite micro/mesoporous molecular sieves. These materials have remarkably high stability, acidity, and catalytic activity due to high acidity and stability of tiny zeolitic fragments and improved accessibility of active sites and transport of bulky reactants and products due to assembling of these fragments into mesostructure. The dimensions of zeolitic fragments depend on the degree of zeolite dissolution, which is in turn governed by the concentration of NaOH in solution used for zeolite destruction. In the extreme case, mordenite phase can be completely dissolved. In the latter case, the catalyst will exhibit the properties of amorphous mesoporous materials.

## CONCLUSIONS

Composite zeolite/mesoporous materials show remarkably high catalytic activity, stability, and selectivity in the transformation of bulky molecules due to high zeolitic acidity combined with improved accessibility of active sites and easier transport of bulky molecules provided by mesopores. The best catalyst performance can be achieved by the optimization of the contributions of micro- and mesopores in the composite material.

## ACKNOWLEDGMENTS

The financial support by Russian Foundation of Basic Research (project 02-03-32516), Council for the Grants of Russian President (project NSh-1275.2003.3), and INTAS grant (project 03 51-5286) is gratefully acknowledged.

## REFERENCES

1. J. S. Beck, J. C. Vartuli, W. H. Roth, M. E. Leonowicz, C. T. Kresge, K. D. Schmitt, C. T.-W. Chu, D. H. Olson, E. W. Sheppard, S. B. McCullen, J. B. Higgins, J. L. Schlenker. *J. Am. Chem Soc*. **114**, 10834 (1992).
2. C. Kresge, M. Leonowicz, W. Roth, J. Vartuli. U.S. Patent 5098 684, Filed 10 December 1990, Issued 24 March 1992.
3. R. Dutartre, L. C. Menorval, F. Di Renzo, D. McQueen, F. Fajula, P. Schulz. *Microporous Mater.* **5–6**, 311 (1996).
4. H. Ajot, J. F. J. Lynch, F. Raatz, P. Caullet. *Stud. Surf. Sci. Cat*. **62**, 583 (1991).
5. D. McQueen, B. H. Chiche, F. Fajula, A. Auroux, C. Guimon, F. Fitoussi, P. Schulz. *J. Catal.* **161** (2), 587 (1996).
6. C. H. Jacobsen, C. Madsen, J. Houzvicka, I. Schmidt, A. Carlsson. *J. Am. Chem. Soc.* **122**, 7116 (2000).
7. A. Karlsson, M. Stöcker, R. Schmidt. *Microporous Mesoporous Mater.* **27**, 181 (1999).
8. S. P. Naik, A. S. T. Chiang, R. W. Thompson, F. C. Huang, H.-M. Kao. *Microporous Mesoporous Mater.* **60**, 213 (2003).
9. L. Huang, W. Guo, P. Deng, Z. Xue, Q. Li. *J. Phys. Chem*. **104**, 2817 (2000).
10. Y. Liu, W. Zhang, T. J. Pinnavaia. *Angew. Chem., Int. Ed.* **40**, 1255 (2001).
11. W. Guo, C. Xiong, L. Huang, Q. Li. *J. Mater. Chem.* **11**, 1886 (2001).
12. Y. Liu and T. J. Pinnavaia. *Chem. Mater*. **14**, 3 (2002).
13. J. Agundez, I. Diaz, C. Marquez-Alvarez, E. Sastre, J. Perez Pariente. *Stud. Surf. Sci. Catal.* **142**, 1267 (2002).
14. Y. Liu, W. Zhang, T. J. Pinnavaia. *J. Am. Chem. Soc*. **122**, 8791 (2000).
15. Y. Di, Y. Yu, Y. Sun, X. Yang, S. Lin, M. Zhang, S. Li, F.-S. Xiao. *Microporous Mesoporous Mater.* **62**, 221 (2003).
16. Y. Goto, Y. Fukushima, P. Ratu, Y. Imada, Y. Kubota, Y. Sugi, M. Ogura, M. Matsukata. *J. Porous Mater*. **9**, 43 (2002).
17. K. R. Kloestra, H. van Bekkum, J. C. Jansen. *Chem. Commun*. 2281 (1997).
18. D. T. On and S. Kaliagine. *Angew. Chem., Int. Ed*. **40**, 3248 (2001).
19. D. T. On, D. Lutic, S. Kaliagine. *Microporous Mesoporous Mater.* **44**, 435 (2001).
20. D. T. On and S. Kaliagine. *Angew. Chem., Int. Ed*. **41**, 1036 (2002).
21. K. Miyazawa and S. Inagaki. *Chem. Commun*. 2121 (2000).
22. P. Van der Voort, P. I. Ravikovitch, K. P. De Jong, A. V. Neimark, A. H. Jansen, M. Benjelloun, E. Van Bavel, P. Cool, B. M. Weckhuysen, E. F. Vansant. *Chem. Commun*. 1010 (2002).
23. A. Corma, U. Diaz, M. E. Domine, V. Fornes. *Angew. Chem., Int. Ed*. **39**, 1499 (2000).

24. N. S. Nesterenko, S. E. Timoshin, A. S. Kuznetsov, I. I. Ivanova, V. Montouillout, F. Thibault-Starzyck, J. P. Gilson, F. Fajula. Proceedings of 14th International Zeolite Conference, Cape Town, South Africa, 2163 (2004).